Rare Metal Materials and Engineering
Volume 53, Issue 7, July 2024
Available online at www.rmme.ac.cn

Science Press

Cite this article as: Zheng Deyu, Xia Yufeng, Teng Haihao, et al. Multi-object Optimization of Forging Process Parameters for Super Large Turbine Disc Based on Taguchi Method[J]. Rare Metal Materials and Engineering, 2024, 53(07): 1887-1896. DOI: 10.12442/j.issn.1002-185X.20230637.

ARTICLE

Multi-object Optimization of Forging Process Parameters for Super Large Turbine Disc Based on Taguchi Method

Zheng Deyu, Xia Yufeng, Teng Haihao, Yang Wenbin, Yu Yingyan

College of Materials Science and Engineering, Chongqing University, Chongqing 400044, China

Abstract: The forging load of super large turbine disc with a diameter over 2 m may approach or even surpass the limit of 800 MN of the largest press machine in China, which is the extreme manufacturing. Thus, maintaining good mechanical properties and controlling forging load are two key factors during the forging process of super large turbine disc. 25 groups of forging parameters was designed based on Taguchi method. The multi-objective optimization of finite element method simulation results was conducted by SNR and ANOVA methods. Results show that the most uniform and refined recrystallization microstructures are obtained under optimal forging load. The optimal combination of process parameters is determined under extreme manufacturing condition: temperature=1120 °C, strain rate=0.06 s^{-1}, pre-forging size=985/610/475 mm, and die temperature=280 °C. The order of importance of each parameter to the simulation results is as follows: temperature>strain rate>billet shape>>die temperature. The experimental results obtained under the optimal parameters combination show good agreement with the simulated results, which demonstrates that this approach may be used to manage the load and microstructure of super large forgings while avoiding a significant number of experiments and numerical simulations.

Key words: multi-objective optimization; FEM; extreme manufacturing; microstructure; load

As one of the largest deformed superalloy disk forgings in the world today, the super large turbine disk forging is an essential part of the class F heavy gas turbine, whose size and structure bring significant technical challenges to the melting, casting, cogging, and hot forging processes. Turbine disk forging has become a real extreme manufacturing from the perspective of equipment capabilities globally when the diameter exceeds 2000 mm[1]. The microstructure and properties of turbine disk forgings exhibit a declining trend as the disk size increases against the background of the upper limit of equipment capacity, and get even worse when approaching the upper limit of equipment load. Therefore, a challenge that needs to be tackled is the multi-object optimization of process parameters that takes into account the equipment capacity, the product microstructure, and the manufacturing cost[2].

The traditional method of "trial and error" experiments to obtain better product properties is expensive and time-consuming, especially for the large forgings made of expensive nickel based superalloy[3], and this cost is unacceptable. The optimal parameter combination cannot be identified by this method since the combinations of parameters cannot be fully applied in the actual manufacturing operation. Therefore, it is necessary to find a theoretical technique that can directly promote the optimal parameter combination selection. As many researches have been conducted, the combination of finite element model (FEM) and optimization technology can be used to optimize process parameters[4]. FEM simulation can predict the results, including forging pressure and microstructure, and optimization technology can compare the simulation results quantitatively under different conditions. In this way, the efficient control of process parameters is realized, and the best configuration within the range of variable parameters is obtained. The application of the theoretical method in the actual manufacturing has greatly saved the cost compared

Received date: October 12, 2023
Foundation item: National Key R&D Program Project Topic (2022YFB3705103); Fundamental Research Funds for the Central Universities (2023CDJXY-020); Chongqing Natural Science Foundation General Project (cstc2021jcyj-msxmX1085)
Corresponding author: Xia Yufeng, Ph. D., Professor, College of Materials Science and Engineering, Chongqing University, Chongqing 400044, P. R. China, E-mail: yufengxia@cqu.edu.cn

with experimental method[5].

Recently, the most widely used multi-objective optimization techniques for process parameters are: FEM combined with Taguchi optimization method[6–8], processing maps optimization method[9–10], Kriging optimization method[11], genetic algorithm optimization[12], particle swarm optimization optimization[13], etc. There are relatively few studies on the optimization of the forging process parameters of the turbine disk, and the studies on the optimization of the extreme manufacturing parameters of the super large turbine disk are rarely stated. Gao[14] created a sensitivity analysis approach for flow behavior, temperature, and microstructure optimization throughout the forging process. This approach can achieve more consistent and finer grain size, reduced flash, and full cavity filling. Stanojevic[15] studied the connection between abnormal grain growth and post-dynamic recrystallization of turbine disk. Laser ultrasonic testing, metallographic analysis, and other methods were used to illustrate the process of grain coarsening caused by post-dynamic recrystallization. To examine the effect of solution annealing parameters on grain coarsening, the post-dynamic recrystallization rate parameter was introduced.

The expense of conducting production tests in extreme conditions is significantly higher than in regular conditions. Therefore, in order to balance and to control the load, mass, and microstructure of super large forgings under extreme manufacturing conditions, it is especially important to find an effective process optimization technique. The maximum cost savings can only be achieved through theoretical optimization in advance. Unfortunately, the application of the proposed multi-object optimization methods in extreme manufacturing conditions has seldom been reported. This study provided a reliable optimization method for multiple process parameters design to achieve the optimal parameters combination under harsh limit conditions of extreme manufacturing. FEM simulations were used to provide simulation data, including load, microstructure, disk diameter, and parameter distribution field, based on the Taguchi method for orthogonal experimental design. The signal to noise ratio (SNR) evaluation method was used to discover the optimal design, and analysis of variance (ANOVA) method was used to find the contribution ratios. The ideal configuration objects were achieved when objective function was driven by the maxima of diameter, the minima forging load (F), average grain size (AVG), and standard deviation (SD) of grain size distribution. The proposed approach can be used in the design of second heat billet for super large turbine disk.

1 Method

The basic method and procedure for the multi-object optimization of super large turbine disk forging are shown in Fig. 1. First, the object function for evaluating microstructure uniformity and refinement is defined[6–7]. Second, the acceptable range of process parameters variables is selected. The optimal range of each parameter variable in extreme manufacturing condition is smaller, and the coupling effect of multiple process parameters needs to be investigated. The best fluctuation range for each parameter was established based on the researches of previous studies[16], after which the factor level and orthogonal test design were constructed. Third, the multiple orthogonal test models of two-dimensional turbine disc are imported into FEM. At the same time, the constitutive equation and microstructure model are implemented into the finite element code[16], and the boundary and load conditions are defined. Finite element simulations run in sequence according to the arrangement order of orthogonal array. Fourth, the simulation results are analyzed to investigate the influence of parameter field distribution, and then the results are transformed into SNR to determine the optimal parameter combination. To determine how each parameter affects the outcomes, ANOVA is carried out. In order to verify the chosen parameters combination, confirmation experiments are lastly carried out.

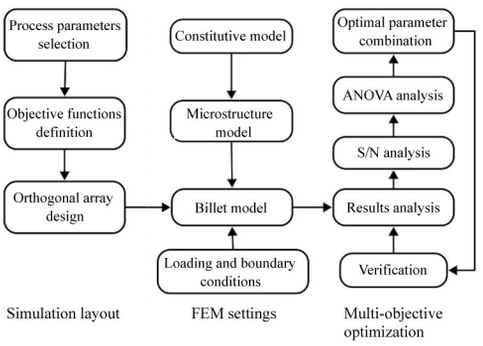

Fig.1 Schematic of process parameters optimization for large forgings

2 FEM Simulations of Super Large Turbine Disk

2.1 FEM modeling

2.1.1 Detail settings

The billet is made of GH4706 superalloy. The initial microstructure, whose initial AVG is about 66 μm, is shown in Fig. 2. In this study, the FEM model of the super large turbine disk is created by DEFORM-2D software using the reverse process parameter design of the two heats process. As shown in Fig. 3, the upper part shows the 3D model of the turbine

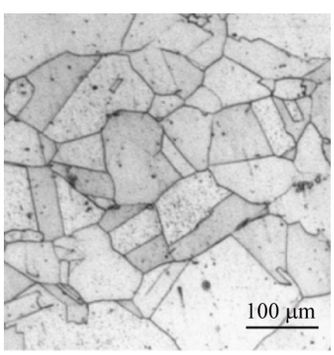

Fig.2 Initial microstructure of GH4706 superalloy

disk for two heats (Fig.3a), while the lower part shows the 2D model of the secondary heat and its section size variables (Fig. 3b). The process conditions in FEM simulation are as follows. (1) The elastic deformation can be ignored due to the high temperature and large deformation in the process. The billet is set to plastic, and two dies are set to rigid. (2) The friction between billet and dies are set to shear type. (3) Ambient temperature is set to 20 °C. (4) The initial section of the billet contains about 5000 elements, and the automatic meshing technique is adopted. (5) The constitutive model and microstructure model of GH4706 superalloy are implanted[16], with 66 μm in initial AVG from experimental measurement, and the grains are uniformly distributed in the billet. (6) The equilibrium equation, geometric equation, volume invariance, and Mises yield criterion are satisfied. (7) Heat transfer and microstructural evolution are taken into account in the process of forging simulation.

2.1.2 Mesh independence verification

The numbers of mesh in FEM simulation will affect the simulation results sometimes. In order to avoid this situation, it is necessary to compare and to verify the output results under different mesh numbers conditions, which is called mesh independence verification[17]. The numbers of mesh in this study are chosen as 1000, 3000, 5000, 7000, and 9000 for independence verification, as shown in Fig. 4. It can be seen that the selection of the mesh number has negligible influence on the output results, which means that there is good mesh independence.

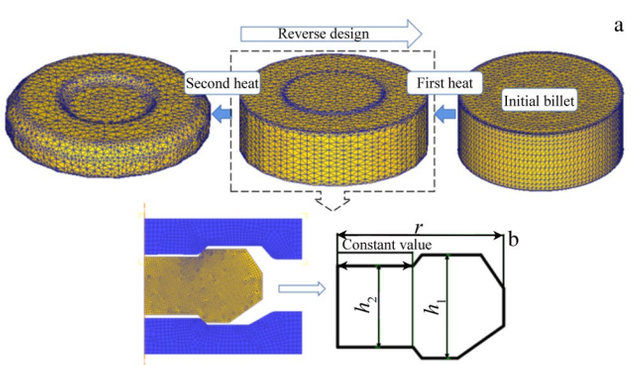

Fig.3 Meshed FEM model of 3D (a) and 2D (b)

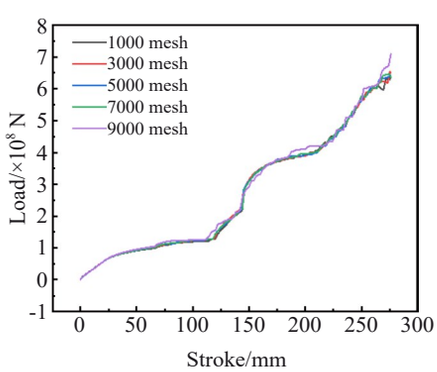

Fig.4 Load-stroke results for different numbers of mesh

2.2 Object functions definition

The stability of the equipment during the loading process can be greatly improved by keeping the maximum forging force as far away from the upper limit of the equipment as possible. This can not only prolong the service life of the equipment and reduce the probability of equipment failure, but also reduce the degradation probability of microstructure and properties of the billet due to unstable loading. Therefore, the maximum forging force is chosen as the optimization object. The ideal compromise point needs to be found because the maximum forging force (the smaller the better) and the diameter of the disk (the larger the better) are contradictory. It has been found that the forging force shows a sharp acceleration when it is close to the upper limit of the equipment, so the forging force at the point before sharp acceleration can be identified as the optimal load, as shown in Fig. 5a. The optimal load F is equal to the total force of all element nodes in contact with the upper die along the Z direction, which can be expressed as:

$$F = \sum_{i=1}^{n} \sigma_{iz} s_{iz} \tag{1}$$

where σ_{iz} is the maximum stress in Z direction of the ith billet element in contact with the upper die, s_{iz} is the contact area of the ith billet element in Z direction in contact with the upper die, and n is the total number of billet elements in contact with the upper die.

High mechanical performances are necessary for turbine disk, which depend on the microstructure. The second

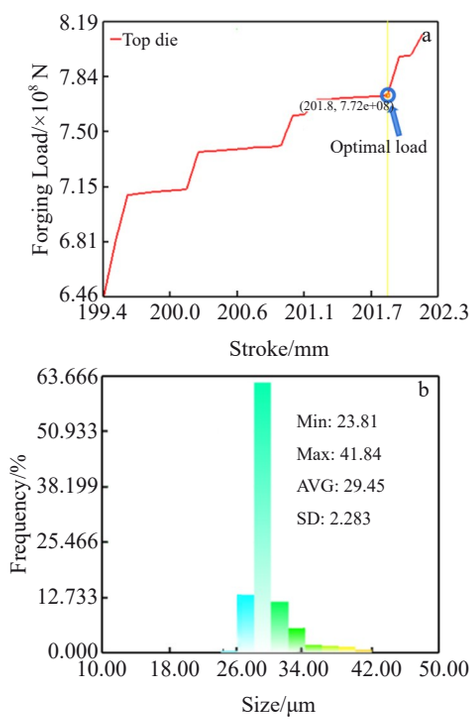

Fig.5 Prediction of forging load (a) and AVG and SD (b) of GH4706 superalloy turbine disk

optimization object is the microstructure. Dynamic recrystallization (DRX) is the primary way of grain refinement for nickel based alloys[16]. Therefore, the object has two aspects, the AVG and the grain attribution uniformity, which is measured by SD, as shown in Fig.5b. The grain size of each element varies and is independent of the element number due to the discretization and non-uniform deformation behavior of FEM simulation. The AVG in Fig.5b refers to the total average value of all grain sizes (including recrystallization and non-recrystallization) under the total volume, and SD represents the overall distribution and fluctuation of grain size inside the total volume. The object functions of AVG and SD under optimized load are expressed as follows:

$$\mathrm{AVG}=\frac{\sum_{i=1}^{m}\int d_i \mathrm{d}V_i}{\sum_{i=1}^{m}\int \mathrm{d}V_i} \tag{2}$$

$$\mathrm{SD}=\left[\frac{\sum_{i=1}^{m}\int \left(d_i-D\right)^2 \mathrm{d}V_i}{\sum_{i=1}^{m}\int \mathrm{d}V_i}\right]^{\frac{1}{2}} \tag{3}$$

where m is the total element number of billet and d_i is the actual AVG of each element in the simulation.

In addition, two further optimization objects, the diameter of turbine disk and the mass of billet (the larger the turbine disk's diameter, the better; the smaller the billet's mass, the better), were focused in this study while considering the product performance and cost.

2.3 Parameter variable selection and orthogonal experimental design

We studied the design of turbine disk pre-forging using the optimization method proposed above. The major variables influence the objects output of turbine disk, including the shape parameters of billet (the radius r, external height h_1, and internal height h_2), strain rate $\dot{\varepsilon}$, billet forging temperature T_1, and die preheating temperature T_2. The placement shape and corner form of the billet are determined by the die shape, which is fixed, and the shape parameters are shown in Fig.3. Due to the load limit of press (the strain rate cannot be too high and the temperature cannot be too low) and the requirements for microstructure (the strain rate cannot be too low and the temperature cannot be too high), the selection ranges of strain rate, strain (i.e. shape), and temperature are very rigorous. Before selecting the parameter range, several simulation tests have been carried out based on the previous research results (as shown in Fig. 6a) to obtain the best parameter selection range (as shown in Fig.6b). The optimal orthogonal test scheme of strain rate, strain, and temperature is obtained within the determined parameter selection range, as shown in Fig. 6b and Table 1. Therefore, the selected parameter range and the obtained optimization results can ensure that the actual optimal parameter combination will not have too many jumps near the optimal parameters.

The volume variation of billet can be controlled by changing the r, h_1, and h_2 of the billet. According to Ref.[16], the optimal strain range for GH4706 is between 0.4 and 0.6, and from the fluctuation range, the shape size is determined, as shown in Table 1. When the ln$Z$ value, where $Z=\dot{\varepsilon}\cdot\exp(52365/T)$[16], is lower than 34 (Fig. 6a), the experimental results show that GH4706 alloy exhibits mixing of multi-level grain size, which is harmful to the mechanical properties of turbine disk. The forging load increases with the rise in strain rate and the reduction in temperature. Therefore, by carefully avoiding mixing of grain size region and minimizing load, the optimal orthogonal tests scheme for strain rate $\dot{\varepsilon}$ and temperature T_1 is obtained, as shown in Fig.6b. The range of T_2 is set to 280–400 °C, considering the temperature tolerance range of steel die. It is decided to use L25 orthogonal tests with 6 factors and 5 levels. The factor-levels are shown in Table 1 and the tests arrangement and results are shown in Table 2, where G is billet mass and R is final forging radius. It can be seen that the results of each

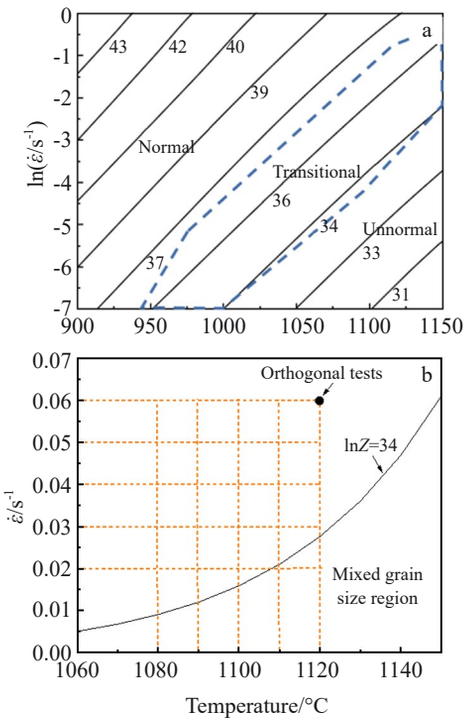

Fig.6 Relationship of ln$Z$ with temperature and logarithm of strain rate[16] (a) and parameters range for orthogonal experimental design (b)

Table 1 Factor-level of parameters

Level	T_1/°C	T_2/°C	$\dot{\varepsilon}$/s^{-1}	Shape parameter/mm		
				r	h_1	h_2
1	1080	280	0.02	970	600	470
2	1090	310	0.03	975	605	475
3	1100	340	0.04	980	610	480
4	1110	370	0.05	985	615	485
5	1120	400	0.06	990	620	490

Table 2 Orthogonal experimental design scheme and simulation results

No.	T_1	T_2	$\dot{\varepsilon}$	r	h_1	h_2	G/t	F/MN	R/mm	SD/μm	AVG/μm
1	1	1	1	1	1	1	11.82	772	1091	2.26	28.9
2	1	2	2	2	2	2	12.05	796	1091	3.31	30.2
3	1	3	3	3	3	3	12.28	724	1093	3.06	28.5
4	1	4	4	4	4	4	12.51	749	1096	2.69	27.5
5	1	5	5	5	5	5	12.75	778	1100	1.85	25.3
6	2	1	2	3	4	5	12.4	792	1098	2.44	30.4
7	2	2	3	4	5	1	12.48	745	1098	2.55	29.5
8	2	3	4	5	1	2	12.41	763	1093	2.79	30.1
9	2	4	5	1	2	3	11.94	785	1089	1.98	27.5
10	2	5	1	2	3	4	12.17	761	1096	2.93	32.7
11	3	1	3	5	2	4	12.53	749	1098	1.94	29.5
12	3	2	4	1	3	5	12.06	785	1094	1.92	29.6
13	3	3	5	2	4	1	12.13	793	1093	2.29	29.5
14	3	4	1	3	5	2	12.36	781	1111	3.21	35.5
15	3	5	2	4	1	3	12.3	739	1097	2.05	31.7
16	4	1	4	2	5	3	12.25	775	1100	2.24	31.9
17	4	2	5	3	1	4	12.18	772	1095	2.37	30.9
18	4	3	1	4	2	5	12.41	789	1140	3.56	37.1
19	4	4	2	5	3	1	12.5	795	1121	2.48	34.2
20	4	5	3	1	4	2	12.03	756	1097	2.52	33.8
21	5	1	5	4	3	2	12.42	762	1104	1.27	29.7
22	5	2	1	5	4	3	12.65	728	1154	1.96	35.1
23	5	3	2	1	5	4	12.17	761	1127	1.98	34.5
24	5	4	3	2	1	5	12.09	770	1107	1.89	32.8
25	5	5	4	3	2	1	12.16	765	1103	3.01	36.1

target show fluctuations and differences. According to the principle that the smaller the G and the larger the F, the better the SD and AVG of grain distribution, and the larger the R, the better. The best schemes for single objective are G (scheme No. 1), F (scheme No. 3), R (scheme No. 22), SD (scheme No. 21), and AVG (scheme No. 5). However, the best scheme must comprehensively consider all objective results, which requires SNR analysis, ANOVA analysis, and weighted SNR analysis, considering the importance of each objective to all simulation results, and the best compromise solution can be obtained by considering all objectives through quantification and comparison.

3 Analysis and Optimization of Simulation Results

3.1 Effect of field distribution on AVG

The values and distributions of temperature, strain, and strain rate have an impact on the evolution and distribution of AVG. To find how the three parameters affect AVG, 25 groups of orthogonal experiments provide the field distribution data for the three parameters, as shown in Fig. 7a – 7c. It can be found that AVG rises with increasing the temperature and strain and decreasing the strain rate. It further shows that AVG exhibits three characteristic regions under the combined effect of temperature fields and strain rate fields. ① Medium AVG appears at "low temperature/low strain rate" field or "high temperature/high strain rate" field. ② Large AVG appears at "high temperature/low strain rate" field. ③ Small AVG appears at "low temperature/high strain rate" field. These conclusions are consistent with previous studies[16].

3.2 SNR analysis

The Taguchi approach converts the results of the FEM analysis into the values of the evaluation characteristics in the optimal parameter analysis by the SNR value rather than the mean value. The major effects of each parameter and its levels on the optimized item can be estimated by this value. The SNR can be defined as follows based on the requirements of the object functions, where Eq.(4) is the smaller the better and Eq.(5) is the larger the better:

$$\frac{S}{N} = -10\lg k_i^2 \tag{4}$$

$$\frac{S}{N} = -10\lg \frac{1}{k_i^2} \tag{5}$$

where k_i is the characteristic value of the ith test. In order to obtain the best process parameters, R should be as large as possible for Eq.(5); G, F, AVG, and SD should be as small as possible for Eq.(4). After FEM simulation and SNR analysis, the multi-object function values and their SNR results under 25 test conditions are calculated, as shown in Table 3.

For each level, the average of the response characteristic

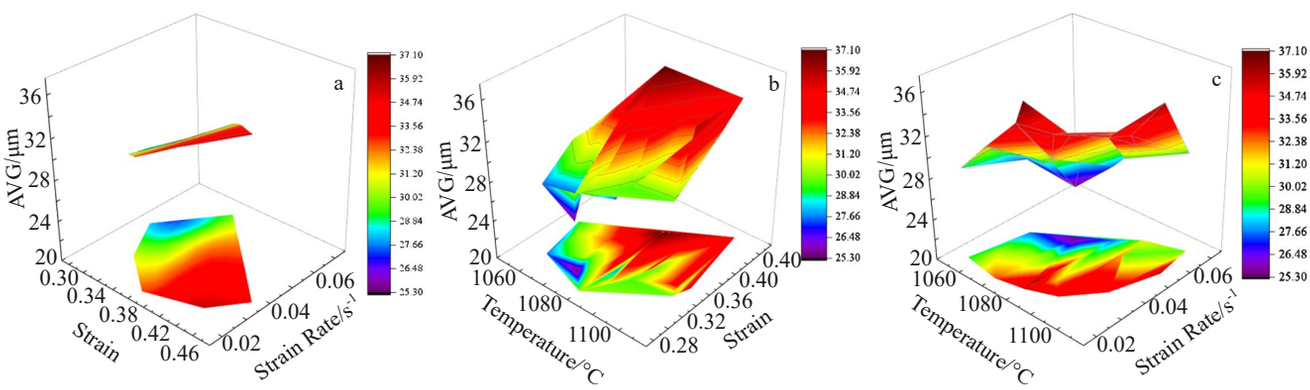

Fig.7 Influence of different parameters on AVG: (a) strain rate and strain, (b) strain and temperature, and (c) strain rate and temperature

Table 3 Multi-object *S*/*N* ratio (dB)

No.	*S*/*N* for *G*	*S*/*N* for *F*	*S*/*N* for *R*	*S*/*N* for SD	*S*/*N* for AVG
1	–21.452	–57.754	60.754	–7.082	–29.218
2	–21.620	–58.018	60.759	–10.397	–29.600
3	–21.784	–57.189	60.772	–9.714	–29.097
4	–21.945	–57.491	60.797	–8.595	–28.787
5	–22.110	–57.818	60.828	–5.343	–28.062
6	–21.868	–57.977	60.816	–7.748	–29.657
7	–21.924	–57.443	60.810	–8.131	–29.396
8	–21.875	–57.652	60.775	–8.912	–29.571
9	–21.540	–57.893	60.739	–5.933	–28.787
10	–21.706	–57.626	60.796	–9.337	–30.291
11	–21.959	–57.487	60.813	–5.756	–29.396
12	–21.627	–57.894	60.779	–5.666	–29.426
13	–21.677	–57.982	60.776	–7.197	–29.396
14	–21.840	–57.853	60.915	–10.130	–31.005
15	–21.798	–57.368	60.804	–6.235	–30.021
16	–21.763	–57.787	60.831	–7.005	–30.076
17	–21.713	–57.748	60.785	–7.495	–29.799
18	–21.875	–57.939	61.136	–11.029	–31.387
19	–21.938	–58.009	60.991	–7.889	–30.681
20	–21.605	–57.567	60.808	–8.028	–30.578
21	–21.882	–57.635	60.859	–2.076	–29.455
22	–22.042	–57.239	61.244	–5.845	–30.906
23	–21.706	–57.625	61.039	–5.933	–30.756
24	–21.649	–57.729	60.882	–5.529	–30.317
25	–21.699	–57.674	60.848	–9.571	–31.150

values is calculated by Eq.(6):

$$\overline{k_i} = \frac{1}{n}\sum_{i=1}^{n} k_i \tag{6}$$

where n is the number of experiments at a certain level. In array L25, n is a constant of 5.

3.3 Multi-object optimization based on method of weighting

For the multi-objective optimization problem in this study, the weighted Taguchi method is used to transform the multi-objective optimization problem into a total objective optimization problem composed of various optimization objectives with different weights for analysis, to investigate the influence of weight distribution on the total optimization result. The weight ratio of each optimization object is calculated according to the importance of each optimization object. The most important objects are the items AVG and SD, which reflect the microstructure of turbine disk, followed by *F*, *G*, and *R*. The multi-object SNR $(S/N)_i$ in the *i*th experiment is defined as follows:

$$\left(\frac{S}{N}\right)_i = \sum_{k=1}^{5} \omega_k \left(\frac{S}{N}\right)_{ki} \tag{7}$$

$$\sum_{k=1}^{5} \omega_k = 1 \tag{8}$$

where $(S/N)_{ki}$ is the *k*th single object SNR in the *i*th experiment, ω_k is the weighting factor of the *k*th single object SNR, and k is the number of optimization objects. Table 4 shows the multi-object SNR with different weighting factor combinations. Three weighting schemes are used for analysis to increase applicability. Table 5 shows the weighted SNR results which are plotted in Fig.8.

The larger the SNR output value of Taguchi method, the smaller the variance between the characteristic value and the expected value, indicating that the scheme is more optimized. Two points can be drawn from the curves in Fig. 8. One is that the shapes of the three curves are consistent, which shows that the weight distribution is independent of the curve shape, that is, independent of the scheme's SNR; the other is the shape of the curve, which indicates that No. 21 (515432) is the best parameters combination, and No. 18 (431425) is the worst parameters combination. This conclusion is consistent with the previous study (Fig. 6b, in

Table 4 SNR weight distribution cases

Case	ω_1 for *G*	ω_2 for *F*	ω_3 for *R*	ω_4 for SD	ω_5 for AVG
1	0.1	0.2	0.1	0.3	0.3
2	0.2	0.2	0.1	0.2	0.3
3	0.1	0.2	0.2	0.3	0.2

Table 5 Average *S*/*N* ratios for three cases (dB)

No.	Case		
	1	2	3
1	–18.511	–19.948	–9.513
2	–19.689	–20.811	–10.653
3	–19.182	–20.389	–10.195
4	–18.828	–20.163	–9.869
5	–17.713	–19.390	–8.824
6	–18.922	–20.334	–9.875
7	–18.858	–20.237	–9.837
8	–19.185	–20.482	–10.151
9	–18.075	–19.635	–9.122
10	–19.505	–20.742	–10.396
11	–18.158	–19.778	–9.137
12	–18.191	–19.787	–9.171
13	–18.664	–20.112	–9.647
14	–20.004	–21.175	–10.812
15	–18.450	–20.006	–9.367
16	–18.775	–20.251	–9.684
17	–18.831	–20.252	–9.772
18	–20.386	–21.471	–11.134
19	–19.267	–20.672	–10.100
20	–19.175	–20.533	–10.036
21	–17.089	–19.069	–8.057
22	–18.553	–20.173	–9.338
23	–18.598	–20.176	–9.419
24	–18.376	–19.988	–9.256
25	–19.836	–21.049	–10.636

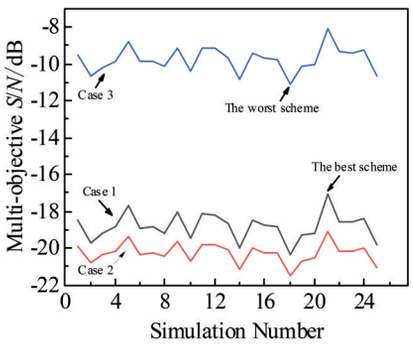

Fig.8 Average SNR of three weight distribution cases

which the No. 18 is located in the mixed grain size region in the lower right corner).

3.4 Contributions of process parameters based on ANOVA analysis

ANOVA is used to assess the influence of process parameters on the object optimization. SS is defined as total square sum of deviation between multi-object SNR and total average SNR, which is used to evaluate the influence significance of process parameters on the optimization objects. The total average SNR can be calculated as follows:

$$\left(\frac{S}{N}\right)_{\text{avg}} = \frac{1}{q}\sum_{i=1}^{q}\left(\frac{S}{N}\right)_i \tag{9}$$

The SS and the ith influencing factor SS_i can be calculated as:

$$\text{SS} = \sum_{i=1}^{q}\left[\left(\frac{S}{N}\right)_i - \left(\frac{S}{N}\right)_{\text{avg}}\right]^2 \tag{10}$$

$$\text{SS}_i = \sum_{j=1}^{p} p\left[\left(\frac{S}{N}\right)_{\text{avg}}^{ij} - \left(\frac{S}{N}\right)_{\text{avg}}\right]^2 \tag{11}$$

where $(S/N)_{\text{avg}}^{ij}$ is the average SNR of the characteristic value of the ith factor at the jth level. The results are shown in Table 6, and its distribution is plotted in Fig.8. The contribution ratio of the ith factor C_i is given by Eq. (12), and the results are shown in Table 7 and plotted in Fig.9.

$$C_i = \frac{\text{SS}_i}{\text{SS}} \times 100\% \tag{12}$$

As can be seen from Fig.9, the average SNR distribution of the characteristic value of the ith factor at the jth level fluctuates in a certain extent, and the overall performance is relatively uniform, which is due to the small range of parameters. The parameter contribution ratios according to the data in Table 6 are calculated further. The influencing degree

Table 6 Average SNR of the ith factor at the jth level

Level of r	No.	k_i	$\frac{S}{N}$	$\left(\frac{S}{N}\right)_{\text{avg}}^{ij}$	Level of h_1	No.	k_i	$\frac{S}{N}$	$\left(\frac{S}{N}\right)_{\text{avg}}^{ij}$	Level of h_2	No.	k_i	$\frac{S}{N}$	$\left(\frac{S}{N}\right)_{\text{avg}}^{ij}$
	1	28.9	–29.218			1	28.9	–29.218			1	28.9	–29.218	
	9	27.5	–28.787			8	30.1	–29.571			7	29.5	–29.396	
970	12	29.6	–29.426	–29.753	600	15	31.7	–30.021	–29.7852	470	13	29.5	–29.396	–29.9682
	20	33.8	–30.578			17	30.9	–29.799			19	34.2	–30.681	
	23	34.5	–30.756			24	32.8	–30.317			25	36.1	–31.150	
	2	30.2	–29.600			2	30.2	–29.600			2	30.2	–29.600	
	10	32.7	–30.291			9	27.5	–28.787			8	30.1	–29.571	
975	13	29.5	–29.396	–29.936	605	11	29.5	–29.396	–30.064	475	14	35.5	–31.005	–30.0418
	16	31.9	–30.076			18	37.1	–31.387			20	33.8	–30.578	
	24	32.8	–30.317			25	36.1	–31.150			21	29.7	–29.455	
	3	28.5	–29.097			3	28.5	–29.097			3	28.5	–29.097	
	6	30.4	–29.657			10	32.7	–30.291			9	27.5	–28.787	
980	14	35.5	–31.005	–30.1416	610	12	29.6	–29.426	–29.79	480	15	31.7	–30.021	–29.7774
	17	30.9	–29.799			19	34.2	–30.681			16	31.9	–30.076	
	25	36.1	–31.150			21	29.7	–29.455			22	35.1	–30.906	
	4	27.5	–28.787			4	27.5	–28.787			4	27.5	–28.787	
	7	29.5	–29.396			6	30.4	–29.657			10	32.7	–30.291	
985	15	31.7	–30.021	–29.8092	615	13	29.5	–29.396	–29.8648	485	11	29.5	–29.396	–29.8058
	18	37.1	–31.387			20	33.8	–30.578			17	30.9	–29.799	
	21	29.7	–29.455			22	35.1	–30.906			23	34.5	–30.756	
	5	25.3	–28.062			5	25.3	–28.062			5	25.3	–28.062	
	8	30.1	–29.571			7	29.5	–29.396			6	30.4	–29.657	
990	11	29.5	–29.396	–29.7232	620	14	35.5	–31.005	–29.859	490	12	29.6	–29.426	–29.7698
	19	34.2	–30.681			16	31.9	–30.076			18	37.1	–31.387	
	22	35.1	–30.906			23	34.5	–30.756			24	32.8	–30.317	

Table 6 Average SNR of the *i*th factor at the *j*th level (continued)

Level of T_1	No.	k_i	$\frac{S}{N}$	$\left(\frac{S}{N}\right)^{ij}_{avg}$	Level of T_2	No.	k_i	$\frac{S}{N}$	$\left(\frac{S}{N}\right)^{ij}_{avg}$	Level of $\dot{\varepsilon}$	No.	k_i	$\frac{S}{N}$	$\left(\frac{S}{N}\right)^{ij}_{avg}$
	1	28.9	–29.218			1	28.9	–29.218			1	28.9	–29.218	
	2	30.2	–29.600			6	30.4	–29.657			10	32.7	–30.291	
1080	3	28.5	–29.097	–28.953	280	11	29.5	–29.396	–29.5604	0.02	14	35.5	–31.005	–30.5614
	4	27.5	–28.787			16	31.9	–30.076			18	37.1	–31.387	
	5	25.3	–28.062			21	29.7	–29.455			22	35.1	–30.906	
	6	30.4	–29.657			2	30.2	–29.600			2	30.2	–29.600	
	7	29.5	–29.396			7	29.5	–29.396			6	30.4	–29.657	
1090	8	30.1	–29.571	–29.540	310	12	29.6	–29.426	–29.8254	0.03	15	31.7	–30.021	–30.143
	9	27.5	–28.787			17	30.9	–29.799			19	34.2	–30.681	
	10	32.7	–30.291			22	35.1	–30.906			23	34.5	–30.756	
	11	29.5	–29.396			3	28.5	–29.097			3	28.5	–29.097	
	12	29.6	–29.426			8	30.1	–29.571			7	29.5	–29.396	
1100	13	29.5	–29.396	–29.849	340	13	29.5	–29.396	–30.0414	0.04	11	29.5	–29.396	–29.7568
	14	35.5	–31.005			18	37.1	–31.387			20	33.8	–30.578	
	15	31.7	–30.021			23	34.5	–30.756			24	32.8	–30.317	
	16	31.9	–30.076			4	27.5	–28.787			4	27.5	–28.787	
	17	30.9	–29.799			9	27.5	–28.787			8	30.1	–29.571	
1110	18	37.1	–31.387	–30.504	370	14	35.5	–31.005	–29.9154	0.05	12	29.6	–29.426	–29.802
	19	34.2	–30.681			19	34.2	–30.681			16	31.9	–30.076	
	20	33.8	–30.578			24	32.8	–30.317			25	36.1	–31.150	
	21	29.7	–29.455			5	25.3	–28.062			5	25.3	–28.062	
	22	35.1	–30.906			10	32.7	–30.291			9	27.5	–28.787	
1120	23	34.5	–30.756	–30.517	400	15	31.7	–30.021	–30.0204	0.06	13	29.5	–29.396	–29.0998
	24	32.8	–30.317			20	33.8	–30.578			17	30.9	–29.799	
	25	36.1	–31.150			25	36.1	–31.150			21	29.7	–29.455	

Table 7 Contribution ratios of the *i*th factor

Variable	SS_i of T_1	SS_i of T_2	SS_i of $\dot{\varepsilon}$	SS_i of billet shape			$(\frac{S}{N})_{avg}$	SS
				r	h_1	h_2		
Value	7.854	0.759	5.216	1.385	0.627	0.739	–29.8726	16.581
Contribution/%	47.37	4.58	31.46	8.35	3.78	4.46	-	-

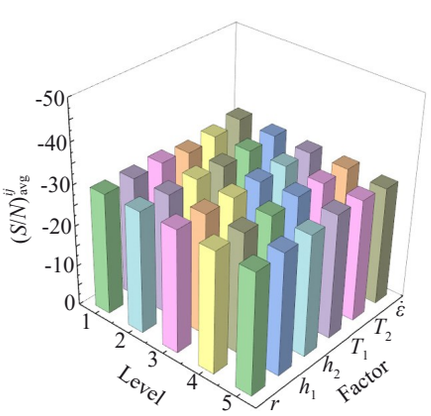

Fig.9 Average SNR distribution of the *i*th factor at the *j*th level

of parameters on the optimization objects ranges as follows: billet temperature T_1 (47.37%)>strain rate $\dot{\varepsilon}$ (31.46%)>billet shape (9.35%+3.78%+4.46%=16.59%) >>die temperature T_2 (4.58%). Among the billet shape variables, radius r has the greatest influence (8.35%), followed by h_2 (4.46%) and h_1 (3.78%). Die temperature has little effect. Therefore, it is possible to design process parameters through this quantitative relationship.

4 Results and Verification

4.1 Simulation verification

It is easy to find from Fig. 8 that the best factor level combination is No. 21 (515432). Forging load, AVG, and SD reach the optimal configuration when the process parameters are T_1=1120 °C, T_2=280 °C, $\dot{\varepsilon}$=0.06, r=985 mm, h_1=610 mm, and h_2=475 mm. FEM simulation results are used to compare the worst scheme No. 18 (431425) with the optimized scheme No. 21, as shown in Fig. 10. Fig. 10a and 10b show that AVG

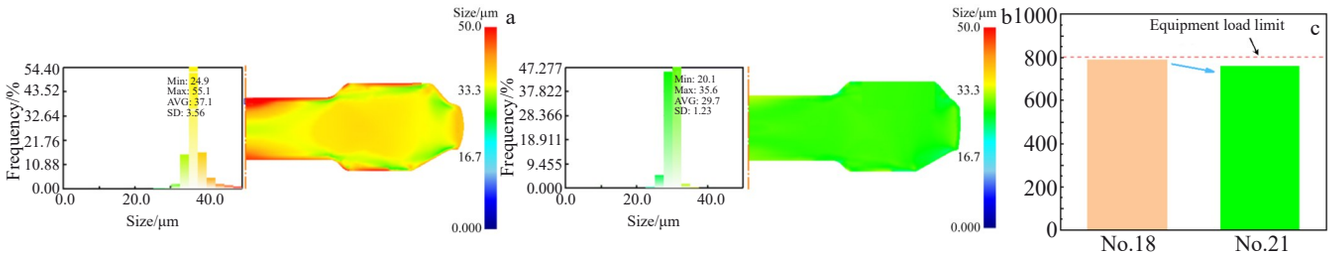

Fig.10 AVG of scheme No.18 (a) and No.21 (b); load *F* of scheme No.18 and No.21 (c)

and SD are considerably optimized from No.18 to No.21, and Fig.10c shows that the load is also reduced. This shows that after SNR and ANOVA analysis of the multi-objective output results of orthogonal schemes, the best scheme obtained has been verified by the simulation results.

4.2 Experiment verification

Isothermal compression tests and microstructure characterization method are used for experimental verification. The tests of standard specimens are conducted using the parameters of No.18 and No.21, based on the simulation results. It can be seen from Fig.11 that coarse grains are generated at the center of disk. Therefore, the compression strain refers to the strain at this position. The strain cloud diagrams of No.18 and No.21 in Fig.11 indicate that the strain of No.18 is slightly greater than that of No.21 near the disk's center. Therefore, strain values of 0.8 (No.18) and 0.7 (No.21) are chosen. It should be noted that these tests only verify the microstructure of local position of the turbine disk at the same strain, and cannot verify the overall microstructure of the turbine disk. However, the test results can also support and prove the effectiveness of this research method in essence. Two samples were cut and wire discharged to dimensions with 8 mm in diameter and 12 mm in height. Each sample is heated to the deformation temperature at a heating rate of 10 K/s and held for 180 s to reduce the anisotropy of flow deformation behavior on a computer-controlled servo hydraulic Gleeble-1500 thermal simulator. It is immediately quenched in water after the compression tests, and the true stress and strain curves are automatically recorded. The microstructure is then scrutinized in the middle to create metallographic diagrams, as shown in Fig.12. The grain size of the metallographic diagrams is calculated and recorded in Table 8.

From Fig.12 and Table 8, it can be observed that No.21 has a more uniform and finer microstructure than No.18, with a relative deviation less than 7%. This study approach can be

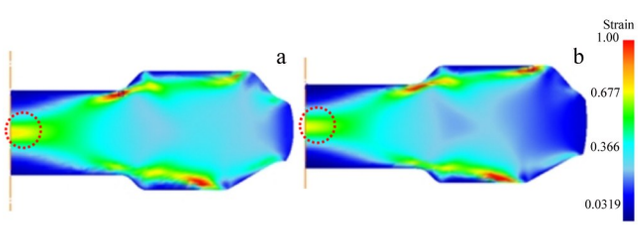

Fig.11 Simulated strain distribution of No.18 (a) and No.21 (b)

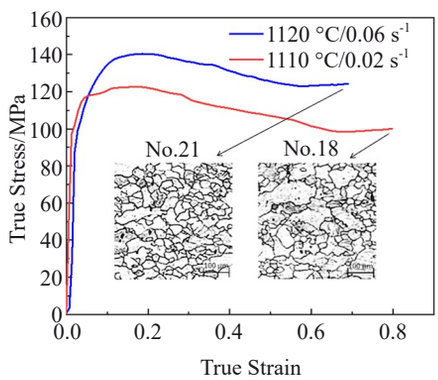

Fig.12 Experimental results of flow stress and microstructure

Table 8 AVG and relative deviation between simulation and experiment results

No.	Parameter	Simulated AVG/μm	Experimental AVG/μm	Relative deviation/%
18	1110 °C /0.02 s^{-1}	37.1	39.6	6.74
21	1120 °C /0.06 s^{-1}	29.7	31.5	6.06

used for multi-objective optimization control of load, and microstructure of GH4706 alloy super large forgings is further demonstrated experimentally by the above.

5 Conclusions

1) The FEM simulation results show that the finest microstructure appears at low temperature and high strain rate field.

2) The influence of SNR weight distribution on the optimization results can be ignored. Three weight distribution schemes show that No.21 (515432, temperature=1120 ° C, strain rate=0.06 s^{-1}, pre-forging size=985/610/475 mm, die temperature=280 ° C) simulation is the best parameter combination to obtain the most uniform and the finest microstructure with the optimal forging load under this condition.

3) The influence degree of the optimization objects ranges in the following orders: billet temperature>strain rate> billet shape>>die temperature. Among the shape variables, radius r has the greatest influence, followed by h_2 and h_1. Die temperature has little effect on the optimization

objects.

References

1 Zhang Rui, Liu Peng, Cui Chuanyong *et al. Acta Metallurgica Sinica*[J], 2021, 57(10): 1215

2 Yao Zhihao, Li Linhan, Zhang Maicang *et al. 8th International Symposium on Superalloy 718 and Derivatives*[C]. Warrendale: TMS, 2014: 129

3 Liu Zhaofeng, Cheng Junyi, Ma Xiangdong *et al. Rare Metal Materials and Engineering*[J], 2024, 53(3): 768

4 Yao Kaijun, Yao Zhihao, Dong Jianxin *et al. Rare Metal Materials and Engineering*[J], 2022, 51(11): 4347 (in Chinese)

5 Jamali A, Nariman-Zadeh N, Darvizeh A *et al. Engineering Applications of Artificial Intelligence*[J], 2009, 22: 676

6 Feng W, Hua L. *Journal of Mechanical Science and Technology*[J], 2011, 25(6): 1519

7 He Xiaoming, Yu Zhongqi, Lai Xinmin *et al. Materials and Design*[J], 2009, 30: 2084

8 Yang Yanhui, Liu Dong, Luo Zijian. *Rare Metal Materials and Engineering*[J], 2011, 40(4): 565

9 Han Yuanfei, Zeng Weidong, Qi Yunlian *et al*. *Materials Science and Engineering A*[J], 2011, 529: 393

10 Wang K L, Lu S Q, Fu M W *et al*. *Materials Characterization*[J], 2009, 60(6): 492

11 Jiang Ping, Cao Longchao, Zhou Qi *et al*. *The International Journal of Advanced Manufacturing Technology*[J], 2016, 86: 2473

12 Xia Qingfeng, Han Jitai. *Materials*[J], 2022, 15: 4607

13 Quan Guozheng, Zhang Yu, Lei Sheng *et al*. *Materials*[J], 2023, 16: 2982

14 Gao Z, Grandhi R V. *International Journal of Machine Tools & Manufacture*[J], 2000, 40: 691

15 Stanojevic A, Bucher C, Gruber M *et al*. *Proceedings of the 9th International Symposium on Superalloy 718 & Derivatives: Energy, Aerospace, and Industrial Applications*[C]. Warrendale: TMS, 2018: 691

16 Huang Shuo. *Microstructure Control and Mechanical Properties Optimization of GH4706 Wrought Superalloy*[D]. Shenyang: Northeastern University, 2015 (in Chinese)

17 Egan B, McCarthy M A, Frizzell R M *et al. Composite Structures*[J], 2014, 108: 963

基于田口法的超大型涡轮盘锻造工艺参数多目标优化

郑德宇，夏玉峰，滕海灏，杨文彬，余盈燕

(重庆大学 材料科学与工程学院，重庆 400044)

摘 要：直径超过2 m的超大型涡轮盘的锻造载荷接近甚至超过了国内最大压力机的极限（800 MN），是真正的极限制造。因此，保持良好的力学性能和控制锻造载荷是超大型涡轮盘热锻生产过程中必须同时兼顾的2个因素。基于田口法设计了25组不同的热锻参数，采用SNR和ANOVA方法对有限元模拟结果进行多目标优化分析，获得了最优锻造载荷和最均匀细化的再结晶组织，确定了极端制造条件下的最佳工艺参数组合（温度1120 ℃，应变速率0.06 s^{-1}，预锻尺寸985/610/475 mm，模具温度280 ℃）。各参数对模拟结果的重要性顺序如下：变形温度>应变速率>坯料形状>>模具温度。使用最佳参数组合获得的实验结果与数值模拟结果吻合较好，表明该方法可以避免大量实验和数值模拟工作量，有效地控制超大型锻件的载荷和微观组织。

关键词：多目标优化；有限元模拟；极端制造；微观组织；载荷

作者简介：郑德宇，男，1983年生，博士，重庆大学材料科学与工程学院，重庆 400044，E-mail：13193805@qq.com